Cell, Vol. 97, 481–490, May 14, 1999, Copyright ©1999 by Cell Press

The Highly Ordered Double-Stranded RNA Genome of Bluetongue Virus Revealed by Crystallography

Patrice Gouet,*# Jonathan M. Diprose,* Jonathan M. Grimes,* Robyn Malby,* J. Nicholas Burroughs,† Stephan Zientara,‡ David I. Stuart,*§‖ and Peter P. C. Mertens†

*The Laboratory of Molecular Biophysics
University of Oxford
Rex Richards Building
South Parks Road
Oxford OX1 3QU
United Kingdom

†Institute for Animal Health
Pirbright Laboratory
Ash Road
Pirbright, Woking
GU24 0NF
United Kingdom

‡Centre National d'Etudes Vétérinaires et Alimentaires
Alfort
Laboratoire Central de Recherches Vétérinaires
22 rue Pierre Curie
BP67
94703 Maisons Alfort Cedex
France

§Oxford Centre for Molecular Sciences
New Chemistry Building
South Parks Road
Oxford OX1 3QT
United Kingdom

Summary

The concentration of double-stranded RNA within the bluetongue virus core renders the genome segments liquid crystalline. Powder diffraction rings confirm this local ordering with a 30 Å separation between strands. Determination of the structure of the bluetongue virus core serotype 10 and comparison with that of serotype 1 reveals most of the genomic double-stranded RNA, packaged as well-ordered layers surrounding putative transcription complexes at the apices of the particle. The outer layer of RNA is sufficiently well ordered by interaction with the capsid that a model can be built and extended to the less-ordered inner layers, providing a structural framework for understanding the mechanism of this complex transcriptional machine. We show that the genome segments maintain local order during transcription.

Introduction

Bluetongue virus (BTV) is the prototype virus species of the genus *Orbivirus*, one of nine genera within the family *Reoviridae*. This large virus family includes many economically important viruses isolated from a wide variety of vertebrates (including humans), invertebrates, and plants, representing a remarkable assortment of viruses. The primary characteristic of the family *Reoviridae* is their genome, composed of 10, 11, or 12 segments of linear dsRNA that are packaged in exactly equimolar proportions.

The icosahedral BTV virion comprises a core particle of two concentric protein layers containing the genomic double-stranded RNA (dsRNA) segments, surrounded by an outer capsid. Like that of other members of the *Reoviridae*, the BTV core remains intact during the early stages of infection and is released into the cytoplasm of the infected cell where it initiates virus replication (the outer capsid is modified or detached on cell entry) (Zarbl and Millward, 1983; Eaton et al., 1990).

Since the viral dsRNAs by themselves would be effectively inert if released as naked RNA into the host cell cytoplasm, the core particles carry viral enzymes into the host cell. These include a transcriptase and helicase, as well as both guanylyl transferase and transmethylase activities required to synthesize, cap, and methylate mRNA copies of the viral genome segments. Even with these enzymes to initiate the processes of transcription and translation, the release of the viral genome would activate host defense mechanisms that could prevent virus replication (Jacobs and Langland, 1996). To avoid such defenses, these viruses retain their genome and enzymes within a protein shell (the core particle), representing a transcriptionally active compartment that separates the dsRNAs from direct contact with the host cell cytoplasm.

However, these aspects of their replication strategy pose significant organizational problems for the *Reoviridae*. First, it is still unknown how the virus manages to select, assemble, and package one copy of each different segment to make up the virus genome. The mechanism is precise, achieving a particle to infectivity ratio as high as 1.0 (Joklik, 1983). It must therefore involve recognition of each segment of the viral genome and have elements of "memory," so that the segments that have already been selected are not incorporated twice (Qiao et al., 1997). The inevitable complexities of such a mechanism may explain why no truly effective reverse genetics system is as yet available for the members of the *Reoviridae* and why the few reports of initial successes use methods that are poorly understood (Roner et al., 1990, 1995; Joklik and Roner, 1996).

Second, each BTV particle contains a total of ten distinct genome segments, each of which is separately and repeatedly transcribed within the confines of the core. The individual dsRNAs must therefore be transported through the active sites of the transcriptase/capping enzyme complexes in such a way that they are recycled ready for the next round of transcription. Data from the orthoreoviruses suggest that transcription of all ten segments can occur simultaneously within a single particle (Gillies et al., 1971). Evidence from the cypoviruses suggests that each genome segment may be specifically

‖To whom correspondence should be addressed (e-mail: dave@biop.ox.ac.uk).
#Present address: CNRS-IPBS, Groupe de cristallographie biologique, 205 route de Narbonne, 31077 Toulouse Cedex, France.

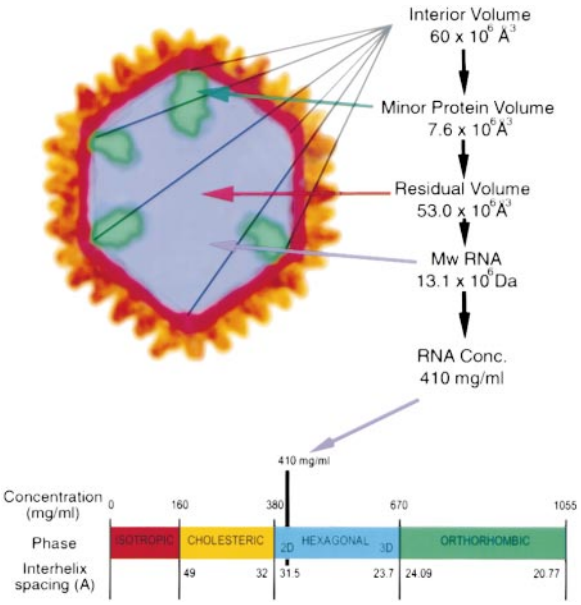

Figure 1. Cartoon of RNA Concentration within the BTV Core

The calculation of the concentration and how it may relate to the defined liquid crystalline phases of different concentrations of dsDNA (incorporating data from Livolant and Leforestier [1996]) is shown. The calculations are described in detail in the text.

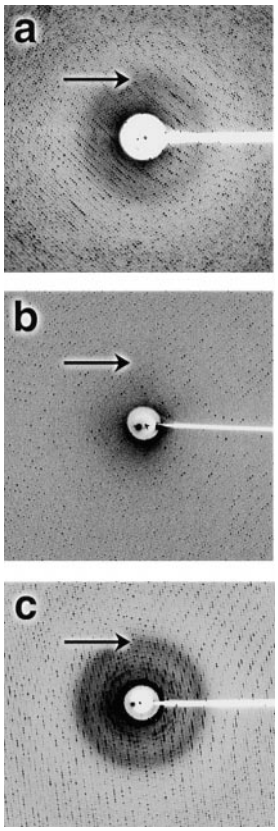

Figure 2. RNA Powder Rings in Low-Resolution Portions of Diffraction Patterns of BTV-1

The arrows mark approximately 30 Å resolution.

(a) Quiescent cores (in standard crystallization liquor) showing a powder ring at a resolution of 30 Å.

(b) Crystals soaked in 25% CsCl, where the ring is lost, presumably due to the contrast matching of the RNA with the mother liquor.

(c) "Activated" particles, soaked in transcription reaction mix as described in the text. Note that the liquid crystalline powder ring is considerably enhanced compared to (a).

associated with a single transcriptase complex (TC) situated at one of the vertices of the intact icosahedral virus particle (Yazaki and Miura, 1980), perhaps explaining why none of the *Reoviridae* possess a genome composed of more than 12 segments of dsRNA (Payne and Mertens, 1983). The independent and simultaneous transcription of the genome segments suggests a high level of organization of the long RNA molecules within the virus core, simply to avoid tangling and steric interference during their movement relative to each other and the TCs.

Because viral genomes are necessarily of lower symmetry than the protein shells, they cannot be structurally resolved by X-ray crystallography except where specifically associated with viral proteins (Namba et al., 1989). In some cases, specific interactions of a relatively small part of the genome (<50%) with defined sites on the icosahedral protein capsid have been visualized (Chen et al., 1989; Macfarlane et al., 1991; Tsao et al., 1991; Fisher and Johnson, 1993; Larson et al., 1993; Tsuruta et al., 1998).

Previous cryoelectron microscopy studies with *Rotavirus* (another genus within the *Reoviridae*) have indicated some ordering of RNA structure in a layer immediately inside the protein capsid (Prasad et al., 1996; Lawton et al., 1997). We describe here the visualization of the majority of a viral genome structure of a larger virus (approximately 80 nm in diameter) within a native and transcriptionally active virus particle, using X-ray crystallography. We present a detailed analysis at 6.5 Å of the internal structures of BTV-1 (Grimes et al., 1998) and BTV-10, the latter determined from crystals for which all three axial lengths exceed 1000 Å. From these and other results, we construct a working hypothesis for the functional organization of the core in its resting state and during transcription. This should provide a paradigm for other members of the *Reoviridae* and shed new light on the problems of genome organization and packaging of dsRNA viruses.

Results and Discussion

Concentration of dsRNA within the Core

From our detailed knowledge of the volume and internal contents, we can calculate the concentration of the dsRNA within the BTV core (Grimes et al., 1998). The total volume of the interior of the core can be calculated from envelopes used in the density modification procedures (see Experimental Procedures) at 60.6×10^6 Å^3. This volume contains the proteins of the transcription complexes. The volume occupied by these proteins can be estimated in two ways, based on the copy numbers (VP1, 12; VP4, 24; and VP6, 72) (Stuart et al., 1998) and molecular masses (VP1, 150 kDa; VP4, 76.4 kDa; VP6, 35.8 kDa) (Roy, 1989b) of the components. First, by using a viral polymerase as a reference (HIV-1 reverse

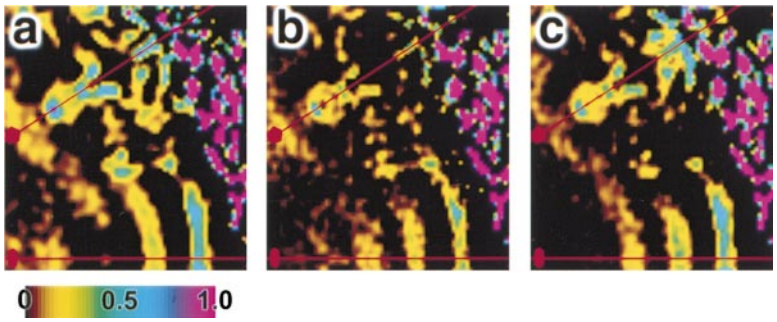

Figure 3. Electron Density Maps for BTV-10 and BTV-1

The color scheme denotes the sigma level of the electron density from 0 to 1, increasing from black to yellow and green to puce, as shown in the color bar. The continuous strong density in an arc to the right of each image is the VP3(T2) shell. Two- (horizontal) and five-fold (diagonal) symmetry axes are marked.

(a) A radial slice through a 60–6.5 Å resolution electron density map for BTV-10. The $2|\mathbf{F}_o|-|\mathbf{F}_c|$ map was calculated using phases derived from the cyclic density modification procedure, in which the RNA of the virus is smoothed, the protein and RNA icosahedrally averaged, and the solvent flattened (see Experimental Procedures for further details). Layers of density can be seen inside the VP3(T2) shell.

(b) A radial slice through a $2|\mathbf{F}_o|-|\mathbf{F}_c|$ 100–6.5 Å resolution electron density map for BTV-1, calculated using phases derived from a similar cyclic density modification procedure to that used to obtain image (a).

(c) Electron density map calculated by cyclic cross-averaging of the BTV-1 and BTV-10 electron density maps (for details, see Experimental Procedures). Figure drawn using EXPLORER (Foulser, 1995).

transcriptase [Ren et al., 1995], volume 127,780 Å^3 for 926 residues), the volume for the TC complexes is estimated as 7.58×10^6 Å^3. Second, using the standard estimate of the packing density (Matthews, 1968) of 0.74 cc/g, the protein volume would be expected to be 7.62×10^6 Å^3. We are therefore fairly confident that the volume of this component of the core will be $\sim 7.6 \times 10^6$ Å^3 (Figure 1). The residual volume for the RNA is therefore $\sim 53.0 \times 10^6$ Å^3. The genome consists of 19,219 base pairs (bp) of dsRNA, with molecular mass $\sim 13.1 \times 10^6$ Da (Roy, 1989a). The concentration of dsRNA within the core is therefore ~410 mg/ml (Figure 1).

The properties of concentrated solutions of dsDNA are relatively well characterized (although less is known about the properties of dsRNA). Thus, it is established that dsDNA forms liquid crystalline arrays at high concentration, with the phase and helix–helix packing distance being a simple function of concentration (Livolant and Leforestier, 1996) (Figure 1). At concentrations of ~400 mg/ml, the liquid crystalline packing arrangement for DNA is shown to be columnar hexagonal, with an interhelix packing distance of approximately 30 Å. We expect the behavior of dsRNA to be similar. One potentially relevant property of this type of structure is that, in the presence of suitable counter ions, the nucleic acid chains can glide over each other with very little friction (Livolant and Leforestier, 1996).

Powder Rings in Diffraction Patterns

If there is a tendency for the genome to form a liquid crystal structure with local ordering of the nucleic acid helices, we might expect that this would be reflected in the way the particles scatter X-rays. In particular, assuming that the ordering is not coherent across the complete crystal lattice, then we might expect to see powder rings manifest in the background scatter of our diffraction images. Figure 2a shows that such a ring is observed in diffraction patterns from quiescent cores, confirming as expected from previous calculations of DNA packing in concentrated solution that there is a tendency for the RNA to form locally ordered structures with strong ~30 Å repeats. Figure 2b presents diffraction from crystals bathed in a concentration of CsCl designed to approximately contrast match the scatter from the dsRNA genome. As expected, the powder ring is no longer visible. We have also addressed the question of what becomes of the RNA during transcription. The cores are transcriptionally active within the crystal; while the crystals remain stable for long periods in reaction mix lacking one or more of the nucleoside triphosphate substrates, they fragment after a few minutes if the full complement of substrates are present. The final panel (Figure 2c) shows the scatter from a crystal immersed in a full reaction mix in the short time window between activation of transcription and destruction of the crystal. We observe that the powder ring is much more prominent than for the resting particle. This may be partly explained by the greater contrast in the less electron-dense reaction mix liquor (0.34 e^-/Å^3) than for the liquor used in Figure 1a (0.37 e^-/Å^3). It does, however, suggest that the local ordering of the liquid crystalline dsRNA genome segments is maintained, or even enhanced, as they move independently within the core during transcription.

The Presence of Counter Ions within the Core

The phosphate backbone of the dsRNA carries a negative charge that is presumably neutralized by counter ions within the particle. We have used a Scanning Proton Microprobe (Grime et al., 1991), situated in the Nuclear Physics Department, Oxford University, to detect the presence of metal ions within the core crystals (see Experimental Procedures). We find that the level of magnesium within the core is too low to be measured, and, while we can detect both calcium and zinc, they are only present at approximately one hundredth of the level of phosphorous. This is insufficient to neutralize the charge on the phosphate backbone and suggests that an organic cation such as spermidine may be present.

Low-Resolution Analysis of Crystals of BTV-10 and BTV-1

As indicated in a previous publication (Grimes et al., 1998), we have observed electron density within the protein shell of BTV-1. To examine the validity of these internal structures, BTV-1 diffraction data were collected to a low-resolution limit of 105 Å, and we determined the structure of a second serotype of BTV, BTV-10, using reflections from 60 Å to 6.5 Å resolution. The

Table 1. Structure Determination Statistics

BTV-10

Resolution (Å)	R_{merge}[a] (%)	Measured Reflections	Unique Reflections	Complete (%)	$\langle I \rangle / \langle \sigma(I) \rangle$	R Factor[b]	Correlation Coefficient[c]
60.0–11.8	23.4	658,898	270,744	83.8	5.81	14.7	94.2
11.8–9.4	32.6	643,606	272,092	85.4	3.62	17.7	90.9
9.4–8.2	48.0	567,707	260,645	82.0	1.89	21.7	85.8
8.2–7.4	66.3	315,246	190,275	60.0	0.98	25.9	76.7
7.4–6.9	73.5	45,229	36,590	11.5	0.74	27.4	68.0
6.9–6.5	71.2	3,612	3,551	1.1	0.84	30.6	54.2
Total	33.6	2,234,298	1,033,897	54.1	2.84	19.5	89.6

BTV-1

Resolution (Å)	R_{merge}[a] (%)	Measured Reflections	Unique Reflections	Complete (%)	$\langle I \rangle / \langle \sigma(I) \rangle$	R Factor[b]	Correlation Coefficient[c]
105.0–11.8	22.4	1,550,615	159,584	98.7	24.8	11.3	96.5
11.8–9.4	25.0	1,343,517	157,802	98.9	22.9	10.1	96.6
9.4–8.2	31.2	1,278,864	157,389	99.0	16.0	11.3	95.8
8.2–7.4	42.8	1,210,838	157,680	99.3	8.80	13.5	94.0
7.4–6.9	49.2	946,711	157,173	99.1	5.35	15.8	91.6
6.9–6.5	49.9	734,199	155,622	98.2	3.81	19.6	87.2
Total	29.9	7,064,744	945,250	98.9	12.6	13.0	95.6

[a] $R_{merge} = \Sigma_j \Sigma_h |I_{j,h} - \langle I_h \rangle| / \Sigma_j \Sigma_h \langle I_h \rangle$, where h are unique reflection indices, $I_{j,h}$ the intensities of symmetry-related reflections and, $\langle I_h \rangle$ the mean intensity (Otwinowski and Minor, 1997).

[b] R factor $= \Sigma_h ||\boldsymbol{F_o}|_h - |\boldsymbol{F_c}|_h| / \Sigma_h |\boldsymbol{F_o}|_h$, where h are the unique reflection indices, $\boldsymbol{F_o}$ the observed structure factors, and $\boldsymbol{F_c}$ the structure factors calculated from inversion of the solvent-flattened map (SHELLSCALE; D. I. S., unpublished program).

[c] Correlation coefficient $= \Sigma_h (\langle |\boldsymbol{F_o}| \rangle - |\boldsymbol{F_o}|_h)(\langle |\boldsymbol{F_c}| \rangle - |\boldsymbol{F_c}|_h) / [\Sigma_h (\langle |\boldsymbol{F_o}| \rangle - |\boldsymbol{F_o}|_h)^2 \Sigma_h (\langle |\boldsymbol{F_c}| \rangle - |\boldsymbol{F_c}|_h)^2]^{1/2}$, where h are the unique reflection indices, $\boldsymbol{F_o}$ the observed structure factors, and $\boldsymbol{F_c}$ the structure factors calculated from inversion of the solvent-flattened map (SHELLSCALE; D. I. S., unpublished program).

BTV-10 structure was determined from crystals containing a whole core particle in the asymmetric unit, with space group $P4_12_12$ and unit cell dimensions 1115 Å × 1115 Å × 1584 Å (see Experimental Procedures). The structure was solved using the molecular replacement method, with the protein capsid of the BTV-1 core structure serving as a phasing model.

As expected, examination of the electron density maps, calculated to equivalent resolutions for the two viruses, indicates that the structures of the capsid are indistinguishable [the amino acid sequences of VP7(T13) and VP3(T2) are 99% identical between the two viruses]. More surprisingly, however, the icosahedrally averaged low-resolution electron density maps of both serotypes show features internal to the VP3(T2) shell that are consistent with layers of dsRNA and are very similar for the two viruses.

Given the unexpected nature of this result, we have used the following protocol to investigate whether the observations are trustworthy. Three parallel analyses were performed, one each for BTV-1 and BTV-10, and one joint refinement simultaneously using the data from both viruses. Initial electron density maps were calculated using phases derived solely from the ordered protein components of the core [780 copies of VP7(T13) and 120 copies of VP3(T2)], and the resolution range used at this point was restricted to 25–6.5 Å. Phase extension was then performed, slowly reducing the low-resolution limit until all data were included, with calculated structure factors substituted where experimental measurements were missing. Features within the core were not only averaged to impose icosahedral symmetry, but also smoothed (by convolution in real space with a Gaussian function) to prevent the buildup of high-frequency noise. The result of this procedure is summarized in Figure 3. The final R factor and correlation coefficient (R and CC; see Table 1 for definitions) for the BTV-1 procedure are R = 13.0% and CC = 95.6%, and for the BTV-10 procedure, R = 19.5% and CC = 89.6%. Cross-averaging between species during the cyclic process results in R = 13.6% and CC = 95.1% for BTV-1 and R = 20.0% and CC = 89.1% for BTV-10. The density features in both maps thought to be RNA are still visible and remain well defined. The real space correlation coefficient [$CC_{real} = \Sigma_x \Sigma_j (\langle \rho_{xj} \rangle \times \rho_{xj}) / \Sigma_x \Sigma_j (\rho_{xj}^2)$, where ρ_{xj} is the electron density at copy j of pixel x, $\langle \rho_{xj} \rangle$ the average density of pixel x, j the sum over BTV-1 and BTV-10, and x the set of pixels within the core envelope (envelope 2) in the Experimental Procedures] was 0.99 in the final round of cross-averaging. The excellent statistics for these analyses suggest that, by the usual criteria, the phase extension process has worked. Electron density maps calculated using the final data from the three experiments are strikingly similar and well defined (Figure 3). We therefore believe that the cross-averaged map provides us with a conservative estimate of the consensus structure within the core (Figures 3c and 4a).

Interpretation of Consistent Density within the Cores of BTV-1 and BTV-10

The electron density distribution that we observe within the cores is consistent with lower resolution electron microscopy analyses of dsRNA viruses (Prasad et al., 1996; Shaw et al., 1996; Dryden et al., 1998) but is more detailed and extensive. The observation of layers is in line with the outer protein shell acting as an external

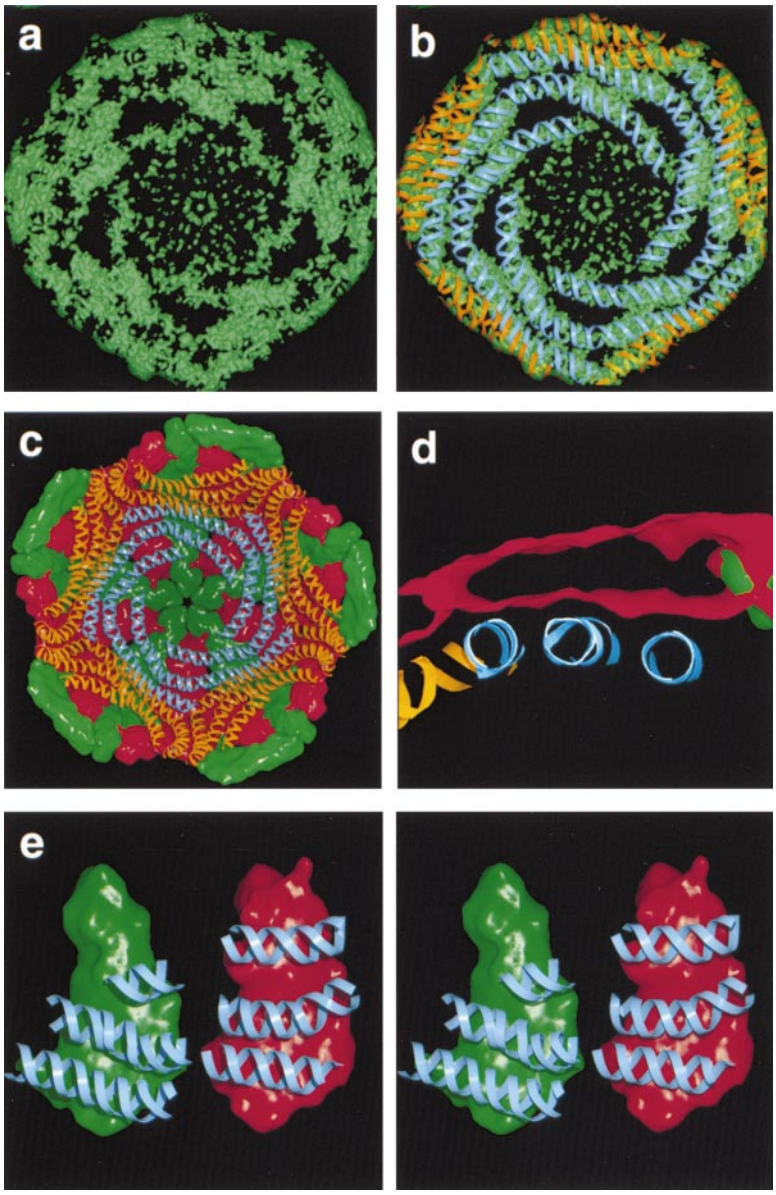

Figure 4. Montage for the Outer Layer of dsRNA

(a) Image of the electron density for the outer layer of RNA, from a map cross-averaged between BTV-1 and BTV-10.

(b) The electron density with A-form RNA modeled into the tubes of density (the phosphate backbone is traced as a blue ribbon for five icosahedral asymmetric units around one of the 5-fold axes). The actual genome cannot follow icosahedral symmetry, so this model has only statistical validity.

(c) The model shown in (b) of the outer layer of dsRNA shown in relationship to the inner surface of VP3(T2). Green and red surfaces are shown for the icosahedrally independent molecules VP3(T2)A and VP3(T2)B, respectively.

(d) Cross-section through the model of the outer layer of dsRNA and VP3(T2), showing the shallow grooves along which the dsRNA tubes tend to align.

(e) A stereo image of the independent molecules of VP3(T2) (A colored green and B red) and the dsRNA model, showing some similarities in the disposition of the dsRNA strands on the two molecules. Figure drawn using BOBSCRIPT (Esnouf, 1997, 1999) and RASTER3D (Bacon and Anderson, 1988; Merritt and Murphy, 1994).

template onto which dsRNA packs, providing a one-dimensional (radial) ordering of the RNA. The separation between the layers is approximately 30 Å, as expected from the observations of powder rings described previously. Figure 4a shows a view of the electron density of the outer layer of RNA. This reveals that the RNA in this layer possesses strong elements of icosahedral symmetry. The layer appears to be made up of a series of strands with the dimensions of dsRNA helices. In addition to these putative RNA layers, there is electron density surrounding the icosahedral 5-fold axes. This density includes some relatively well-ordered features close to the apical domain of VP3(T2) and shows a variety of features closer to the center of the particle. We assume that these features correspond to the TCs, in part because corresponding features have been observed in cryo-EM studies of members of other genera within the *Reoviridae* (*Rotavirus* [Prasad et al., 1996], *Orthoreovirus* [Dryden et al., 1998], and *Aquareovirus* [Shaw et al., 1996]). The electron density we observe within the core represents the averaged structure of the core particles within the crystals convoluted with the elements of icosahedral symmetry. This will therefore represent a 5-fold averaged version of the structure, preventing us from unraveling a full "wiring diagram" for the RNA. Nevertheless, the surprising clarity of the density, for the outer layer of RNA in particular, implies that the inner surface of the VP3(T2) layer imposes considerable icosahedral order on the packaged genome. The weakening of the electron density toward the center of the core suggests that the RNA becomes more disordered the further it gets from this protein layer.

We have modeled the structure of the RNA. A-form double helices have been fitted into the electron density, with kinks introduced as necessary (Figure 4). Segments of dsRNA were generated and modeled into the density of the protomeric unit using the graphics program TURBO-FRODO (Roussel et al., 1991). The resulting RNA

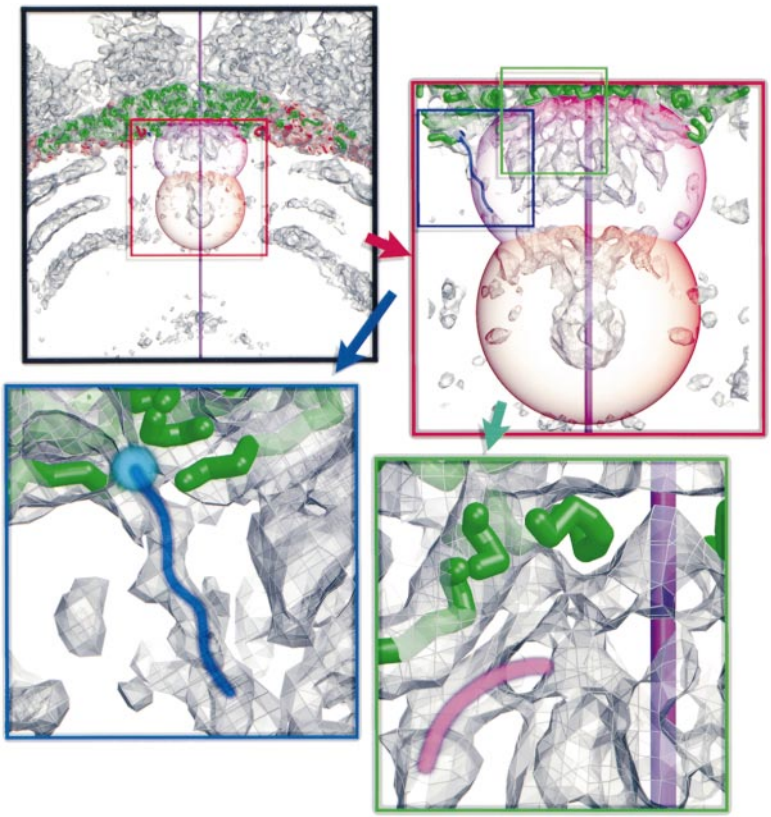

Figure 5. Montage of Elements of the Transcription Complex (TC)

The top left panel shows an overall view of a 5-fold axis (marked vertically as a purple line) along which are density features for the TC and around which the layers of RNA are clearly visible. The transparent orange and mauve geometric objects reflect the volumes that a monomer of VP1 (polymerase) and a dimer of VP4 (capping enzyme) would fill, respectively, assuming standard packing densities. The top right panel shows a close-up of the TC, showing the same geometric objects with the N terminus of the VP3(T2)A molecule marked as a blue stroke. The density for the ordered N terminus is shown in close-up in the bottom left panel. The point where we lose the density in the high-resolution structure of the core (Grimes et al., 1998) is shown as a cyan spot, and the continuation of the density in the low-resolution map is marked as a blue line. The bottom right panel shows a close-up of the electron density where a well-ordered portion of the capping enzyme (VP4, marked with a pink stroke) packs against VP3(T2)A, residues 307–328. Figure drawn using BOBSCRIPT (Esnouf, 1997, 1999) and RASTER3D (Bacon and Anderson, 1988; Merritt and Murphy, 1994).

model was energy minimized in X-PLOR (Brünger, 1992), simply to relieve kinks. Individual tubes of density spiralling around the 5-fold axes are most clearly visible in the outer layer, which has been modeled as three pieces of dsRNA ranging in length from 32 to 55 bp. There are connections between these spirals, presumably representing different possible paths for the RNA in each icosahedral asymmetric unit and within the viral population as a whole. RNA has been modeled into the tubes and the strongest connections. Consequently, these modeled strands clash in several places, in particular between icosahedrally related copies. The icosahedral asymmetric units of the second and third layers have each been modeled by two pieces 33–53 bp in length and the inner layer as a single 43 bp length. This model has not been refined against the diffraction data, since such a procedure would not eliminate the most serious limitations in the model, the chemical inconsistencies arising from icosahedral averaging. Despite the weakening of the electron density toward the center of the core, there is some evidence from the electron density that the inner layers possess a spiral organization.

The Organization of RNA Is Partially Ordered by VP3

Our model (when corrected for overlap) represents ~80% of the 19,219 bp of the BTV genome (Roy, 1989a) (total length ~50,000 Å). The model suggested by the electron density implies that there is a particular organization of the various components within the core. Such ordering appears to be imposed by chemically featureless grooves that form tracks for the RNA on the inside of the VP3(T2) layer (Figures 4c and 4d). Specific RNA/protein interactions are evident at only two points in the icosahedral asymmetric unit, involving the long βJ/βK loop (residues 790 to 817, secondary structure defined in Grimes et al. [1998]) in the dimerization domains of the VP3(T2)*A* and VP3(T2)*B* molecules [this loop is partially disordered in VP3(T2)*B* {Grimes et al., 1998}]. Apart from Lys-807 on the βJ/βK loop, there are very few basic residues on the inner surface of VP3(T2). This paucity of specific interactions appears likely to facilitate the movement of RNA within the core, for example during transcription, while the counter ions presumably lubricate the RNA/VP3(T2) interface and the interactions between adjacent RNA layers. The capsid is built up from two structurally distinct copies of VP3(T2) (Grimes et al., 1998). Figure 4e shows that there are some striking similarities in the interactions each of these make with the RNA (there are also differences that reflect specific conformational changes between the two protein subunits). Since the two molecules lie at different radial distances from the TCs at the 5-fold axes, the quasi-equivalence in the protein–RNA interactions generates the observed spiral structure in the RNA.

A Model for the Packing of RNA

We propose a model in which each dsRNA strand in the outer shell of RNA leaves the TC at the 5-fold axis and spirals around it until, at a certain diameter away from the 5-fold axis, it clashes with a neighboring RNA segment. This might redirect the RNA inward to lay down the second discrete layer, spiralling back toward the TC. Further switching would lay down the third and fourth layers. Although no electron density is seen connecting the layers, 5-fold averaging would render a single link

invisible. Since the gene segments are of quite different lengths (from 822 to 3954 bp) and there is very little free space within the particle, some of the longer segments must trespass on the volume of neighboring segments (and on the volume around the two 5-fold axes that are empty of genome). This suggests that simple steric clashes with neighboring segments might be the most important factor limiting the lateral expansion of the spiral, although it is possible that layer switching might be facilitated by interaction with the flexible loop of VP3(T2)*B* bearing Lys-807, close to the icosahedral 3-fold axis.

Organization of the Transcription Complexes

EM analyses of transcribing cores of related viruses (Gillies et al., 1971; Yazaki and Miura, 1980; Lawton et al., 1997) are consistent with the TCs lying at the 5-fold axes of the core and with mRNA being extruded at, or close to, these symmetry axes. In BTV, the electron density indicates that the TCs, which are nonsymmetric, lie along the 5-fold axes of the virus, at the heart of the RNA spirals, and below pores in the VP3(T2) layer (Grimes et al., 1998), which if slightly expanded from the resting structure we see, would allow the exit of the RNA (Figure 5). The volume of the overall envelope of electron density assigned to protein inside the VP3(T2) shell at each of the icosahedral 5-fold axes is $\sim 350 \times 10^3$ Å^3, almost sufficient to accommodate the monomeric VP1(Pol) and two subunits of VP4(Cap), which assuming standard packing densities, would occupy a total of 366×10^3 Å^3 (Figure 1). The N-terminal 50 residues of VP3(T2)A, situated closest to the 5-fold axis, appear to modulate the symmetry mismatch that exists between the 5-fold symmetric VP3(T2) shell and the asymmetric TC. These N-terminal residues swing down [compared to their positions in the VP3(T2)B molecule where they are well ordered {Grimes et al., 1998}] and seem to engage the TC, holding at least some of the enzyme components in the correct orientation. This domain may therefore be key to the structural basis for the TC and RNA organization and the mechanics of RNA synthesis and export from the core. This is consistent with observations for orthoreovirus, where the λ1 protein, the structural homolog of VP3(T2), is enlarged compared to BTV, containing a proteolytically sensitive N-terminal region that is not completely ordered (Smith et al., 1969; White and Zweerink, 1976) and seems to be located (at least in part) close to the icosahedral 5-fold axes (Dryden et al., 1998). We suggest that in BTV, the dimeric protein VP4, which has capping activity (Ramadevi et al., 1998), lies immediately within the VP3(T2) layer, forming strong interactions with residues 307–328 of VP3(T2)A (Figure 5). This would accord with the observation that cores can cap exogenous RNA (Mertens et al., 1992). Internal to VP4, and probably stabilized in part by interactions with the N terminus of VP3(T2)A, lies the monomeric VP1 viral transcriptase (Figure 5).

Conclusions

The peculiar architecture of 120 protein subunits in the layer immediately surrounding the genome appears to be a characteristic of dsRNA viruses (Grimes et al., 1998). The reasons for the conservation of this number are not known, but we expect that they may relate to the evolutionary history of these viruses, perhaps indicating a unique evolutionary accident that produced an enzymatically competent shell capable of sequestering the dsRNA genome. The staggered organization of ten subunits around each 5-fold axis of the icosahedron is reflected in the partial icosahedral order of sections of the dsRNA genome, which is thereby organized into a spiral. The order extends to inner layers of RNA, and this organization may provide a solution to the severe problems dsRNA viruses face in producing an efficient transcriptional machine within the confined space of the virus capsid, as well as choreographing the RNA during the transcription of the genome segments. This process is remarkable, as the ten segments of viral dsRNA are transcribed simultaneously at high speed (up to 50 nucleotides per second in orthoreoviruses [Bartlett et al., 1974]) by the core-associated TCs. The limited flexibility but considerable fluidity of the dsRNA within a liquid crystal structure probably allows the double helices to be pushed, pulled, and spun about their helical axes as required for transcription, while a level of organization is maintained by the VP3(T2) layer and the high RNA concentration. Evidence from the diffuse scattering at 30 Å spacings (Figure 2) shows that local order is indeed maintained within the RNA in the highly active process of transcription. Taken together, our observations lead us to propose the conceptual model for the organization of these viruses shown in Figure 6. Although, as mentioned above, details may vary between different members of the family *Reoviridae*, we expect that many basic features will be conserved.

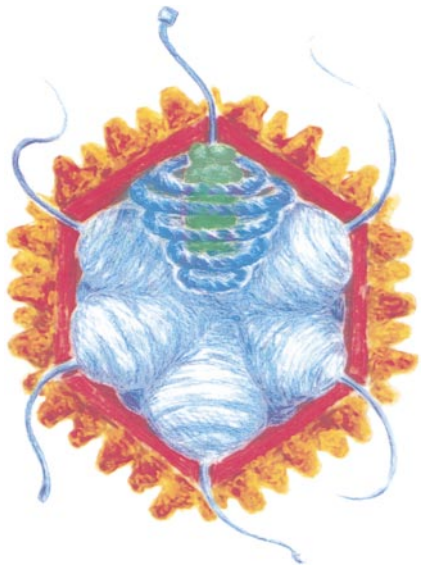

Figure 6. Cartoon of the Model for the Arrangement of the RNA

The RNA is shown as a blue coil around the TC (colored green), indicating the disposition of the RNA within the core with respect to the 5-fold vertices.

Experimental Procedures

Data Collection and Analysis for BTV-10

BTV-10 (USA) was grown and viral cores prepared using established procedures (Mertens et al., 1987; Burroughs et al., 1995). Crystals were grown at 20°C in microbridges. The largest crystals reached

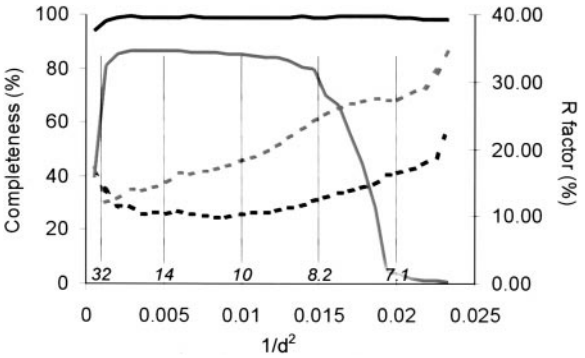

Figure 7. Analyses of the BTV-1 and BTV-10 Data Sets

The graph shows the completeness of the BTV-1 and BTV-10 data sets in black and grey solid lines, respectively, with respect to scattering angle (resolution). The scattering angle is marked as $1/d^2$, where d is the real space resolution, in Å. The corresponding d values are marked above the axis in italics. The merging R factor (as defined in Table 1) is shown as dashed lines (black for BTV-1 and grey for BTV-10).

a diameter of 0.4 mm and are more fragile than BTV-1 core crystals (Burroughs et al., 1995). In the course of the structure determination, it emerged that BTV-10 core crystals belong to space group $P4_12_12$ with cell parameters a = b = 1115 Å, c = 1584 Å. The crystal unit cell contains one core particle in each asymmetric unit. Data collection was at the high brilliance undulator beamline ID2 (BL4) at the European Synchrotron Radiation Facility (ESRF), Grenoble, France. The highly parallel beam, in conjunction with limiting apertures on the incident beam of 50–80 μm and a 30 cm MAResearch imaging plate at 1.05 m from the crystal, allowed the diffraction orders to be resolved at a wavelength of ~1 Å. Careful experimental design allowed relatively low angle diffraction (60 Å resolution) to be collected with reasonable background noise. Crystals were cooled to about 8°C and randomly oriented. Oscillation ranges per image were 0.15°–0.3° with exposure times of 20–40 s. It was possible to obtain two images from some crystals. In total, 100 images from 75 crystals were used (although many more crystals were examined), most with the detector aligned centrally with the beam. However, a third of the images were collected with the detector swung to a 2θ value of 4° or 5°. Images were indexed and integrated with the program DENZO (Otwinowski and Minor, 1997), keeping overlapping reflections. Overlapped reflections were deconvoluted using PrOW (Bourgeois et al., 1998) and the resolution dynamically determined with TRIM-DENZO (D. I. S., unpublished program). Data were scaled and merged with SCALEPACK (Otwinowski and Minor, 1997). An initial run of SCALEPACK determined scale factors; partial intensities with a fraction above 0.5 were scaled up using a program we wrote for the purpose; finally, the data were merged in a second run of SCALEPACK. A unique data set of 1,034,180 reflections was obtained in the range of 60 to 6.5 Å, with a completeness of 54% (84.5% for the 60–11.8 Å shell; see Table 1 and Figure 7). Intensities were converted to structure factor amplitudes using the CCP4 program TRUNCATE (French and Wilson, 1978).

Structure Solution of BTV-10

The phase problem was solved and space group determined using the program X-PLOR (Brünger, 1992) once a preliminary 7.2 Å data set of 901,178 unique reflections was available. A few **h00** reflections were measured, which suggested that the space group was likely to be P4n212, where n was unknown. The particle orientation was determined by inspection of a self-rotation function and confirmed by PC refinement (Delano and Brunger, 1995) of a Cα atom model derived from BTV-1 (Grimes et al., 1998) (an anti-aliasing B factor of 1500 was applied to reduce sampling errors). The space group and particle position were determined by factoring the space group symmetry operators to reduce the problem to 1-D and 2-D searches. Rigid body refinement was combined with a grid search refinement of the unit cell dimensions to give a best solution with a correlation coefficient of 0.72 and R factor of 31% (correlation coefficient = $\Sigma_h(<\mathbf{F_o}>-|\mathbf{F_o}|_h)(<\mathbf{F_c}>-|\mathbf{F_c}|_h)/[\Sigma_h(<\mathbf{F_o}>-|\mathbf{F_o}|_h)^2\ \Sigma_h(<\mathbf{F_c}>-|\mathbf{F_c}|_h)^2]^{1/2}$, R factor = $\Sigma_h||\mathbf{F_o}|_h-|\mathbf{F_c}|_h|/\Sigma_h|\mathbf{F_o}|_h$, where *h* represents the unique reflection indices, $\mathbf{F_o}$ the observed structure factors, and $\mathbf{F_c}$ the structure factors calculated from inversion of the solvent flattened map). The BTV-1 coordinates may be moved into the BTV-10 cell by a translation of 222.0, 990.5, 736.0 Å and a rotation of $\phi_1 = 242.77°$, $\phi_2 = 73.55°$, $\phi_3 = 157.53°$ (X-PLOR [Brünger, 1992] Eulerian angle convention).

A bulk solvent correction (solvent density = 0.25 e/Å^3, B factor = 120, R factor = 30.6%) was applied to the BTV-10 model to give a set of model structure factor amplitudes and phases, $\mathbf{F_c}$. The $\mathbf{F_o}$ were scaled to the $\mathbf{F_c}$ by the application of a scale factor (14.5) and a B factor (−32.0) to give the set of $\mathbf{F_o}$ used in the cyclic density modification. The scale and B factors were calculated from a Wilson plot using only data in the range of 10–6.5 Å, over which our model was thought to be good. The $\mathbf{F_c}$ were then scaled to these $\mathbf{F_o}$ over the resolution range 25–6.5 Å and weighted using the schemes suggested by Rayment (1983) (SHELLSCALE; D. I. S., unpublished program). Unobserved data were included with a weight of 0.7. A $2|\mathbf{F_o}|-|\mathbf{F_c}|$ electron density map was calculated for the same resolution range. This map was the starting point for cyclic density modification.

The Structure Solution of BTV-1

The procedures involved in preparing and growing crystals and the collection of X-ray diffraction data for BTV-1 (SA) cores have been described previously (Burroughs et al., 1995; Grimes et al., 1998). As for the BTV-10 data collection, particular attention was paid to collecting very low resolution reflections through careful experimental design. The data set used for the work presented here differs significantly from that presented previously in three main areas. First, the inclusion of further data improved the completeness of the data set, extended the low-resolution limit from 100 Å to 105 Å, removed the need to use a low-resolution subset of data collected from selenomethionated core crystals, and allowed the use of much stricter checks on data quality. Second, a larger version of SCALEPACK (Otwinowski and Minor, 1997) enabled all 21,568,019 observed reflections to be merged simultaneously. Third, only a 105–6.5 Å subset of the data was used, as little high-resolution information was expected from the interior of the core. Some data processing statistics over this range are shown in Table 1, and a plot of completeness by resolution is given in Figure 7.

A bulk solvent correction was applied to the current atomic model by refinement against the $\mathbf{F_o}$ using X-PLOR (Brünger, 1992) (solvent density = 0.28 e/Å^3, B factor = 100, R factor = 25.32%) to give a set of model structure factor amplitudes and phases, $\mathbf{F_c}$. As with the BTV-10 data, the $\mathbf{F_o}$ were scaled to the $\mathbf{F_c}$ by the application of a scale factor (1.52) and a B factor (−12.9) to give the set of $\mathbf{F_o}$ used in the cyclic density modification. The scale and B factors were calculated from a Wilson plot, again using only data in the range of 10–6.5 Å. The $\mathbf{F_c}$ were then scaled to these $\mathbf{F_o}$ over the resolution range 25–6.5 Å and Rayment weighted (Rayment, 1983). Unobserved data were included with a weight of 0.7. A $2|\mathbf{F_o}|-|\mathbf{F_c}|$ electron density map was calculated for the same resolution range. This map was the starting point for cyclic density modification.

Density Modification Procedures

For both BTV-1 in the orthorhombic space group $P2_12_12$ (cell parameters a = 795 Å, b = 821.5 Å, c = 753 Å) (Grimes et al., 1998) and BTV-10 in the tetragonal space group $P4_12_12$ (cell parameters a = b = 1115 Å, c = 1584 Å), layers of diffuse electron density were present beneath the inner shells of VP3(T2). To obtain the clearest possible image of these layers and to ensure that they were not artifacts, cyclic averaging of the electron density was performed independently for the two crystal forms, during which the electron density inside the VP3(T2) protein shell was smoothed.

Envelope Determination

For BTV-1 and BTV-10, the procedures were essentially identical. For a cyclic averaging and density modification procedure, envelopes must be designed that delineate those regions of the asymmetric unit within which the local symmetry operators are believed

to be valid. For the more complex procedure used here, envelopes were constructed to define (1) the volume internal to the core capsid, (2) the entire core, and (3) the solvent region of the crystallographic asymmetric unit. These envelopes were built up in a series of steps, and (1) and (2) were defined over the appropriate asymmetric volume of the virion (1/2 particle for BTV-1 and 1 particle for BTV-10). An envelope defining the core capsid in the asymmetric volume was first generated using a modified version of the algorithm of Wang (1985) (program GAP; D. I. S. and J. M. G., unpublished). A sphere of radius 360 Å centered on the particle was used to cut away crystallographically related viruses. Relatively simple logical operations were then used to define the various compartments listed above. These envelopes were redefined after every 15 cycles of density modification.

Density Modification Protocols

For the density modification procedure, three operations were carried out. First, using the envelope which defined solely that volume internal to the capsid (envelope 2), the "RNA" electron density in the expanded map was convoluted with a Gaussian weighting function whose width was determined by a B factor. The B factor used in these density modification experiments was 20 $Å^2$. This was done to prevent overfitting of the higher resolution data. By working in real space, we can easily assign different characteristics to the power spectrum of different regions of the electron density, something that would be very difficult to accomplish in reciprocal space. The entire core (envelope 2) was then averaged using noncrystallographic symmetry (NCS) operators defining the icosahedral symmetry of the capsid. A double interpolation method was used to reduce computation time. The smoothed/averaged density for the core was then folded back down into the asymmetric unit of the crystal, with the solvent regions of the map (envelope 3) flattened. This smoothed/averaged and solvent-flattened representation was then used to obtain calculated amplitudes and phases, which were merged with the observed data, with calculated data inserted for unobserved reflections to attenuate series termination effects. These merged data were then scaled in resolution shells (SHELLSCALE; D. I. S., unpublished program) and weighted according to Rayment (1983) before the calculation of a new $2|\mathbf{F_o}|-|\mathbf{F_c}|, \alpha_{\text{current map}}$ electron density map to complete a cycle of refinement. Ninety cycles of density modification were performed, with the Rayment weighting scheme replaced with unit weights for the final twenty-five cycles.

In order to escape the limitations of our model at low resolution, low-resolution phase extension was performed (SHELLSCALE; D. I. S., unpublished program). The low-resolution limit (D_{min}) was initially set to 25 Å. This was increased to

$$\frac{1}{{}^1/_{D_{min}} - {}^1/_{1600}}\ Å$$

each cycle, reaching $D_{min} = 1600$ Å after 63 cycles. D_{min} remained at this value for the remaining cycles, including all terms except the (000) in the map calculations for both BTV-1 and BTV-10.

When phase refinement converged, the maps for both BTV-1 and BTV-10 contained clear layers and, in some places, tubes of density corresponding to dsRNA. There was a strong correspondence between the two independent determinations (Figures 3a and 3b).

Cross-Averaging Procedures

As a final check of these features and to obtain the best image possible, these cyclic density modification procedures were rerun in parallel, with the inclusion of a cross-averaging step after the end of the other density modification procedures. The two maps were scaled together based on the icosahedrally averaged protein regions. The crystallographic asymmetric portion of the core was then averaged between the two maps and the resultant density placed back into the solvent-flattened asymmetric unit. This was done both in BTV-1 and BTV-10 space in order to minimize interpolation errors. These cross-averaged maps were fed back into the cyclic procedure described above. The extra constraints applied by the cross-averaging allowed the convolution step to be discarded.

Scanning Proton Microprobe

The scanning proton microprobe is capable of detecting atoms heavier than neon at a level as low as 10 ppm through proton-induced X-ray emission of characteristic wavelengths. The atomic composition was determined from an intensity spectrum (Grime et al., 1991).

Crystals of BTV-1 cores were first inactivated by subjecting them to 56°C for 120 min. They were then fixed in 0.25% glutaraldehyde solution for 30 min, washed twice for 1 min in deionized water, and mounted on a layer of Mylar 2 μm thick. Spectra were collected at three positions from the crystal that best survived this process. As the only source of phosphorous was the dsRNA, the concentrations of each atom were normalized by conversion to mol/mol phosphorous. Based on consideration of the amino acid compositions and number of base pairs of RNA, the expected relative amount of sulphur was 0.62. The observed mean sulphur level of 0.59 indicated that the washes had succesfully removed the 25% saturated ammonium sulphate present in the crystallization buffer and by implication any other ions not bound by the core.

Acknowledgments

We thank the SRS, ESRF, and EMBL for their assistance in data collection, in particular the staff of ID2 at the ESRF; the disease security officers D. Goodridge, S. Williams, A. Meyer, and P. Wilkinson; M. Pickford for technical assistance; R. Bryan, K. Measures, and R. Esnouf for computing; S. Lee for assistance with figures; and P. Roy and E. Y. Jones for discussion. This work has been given long-term support by the Biotechnology and Biological Sciences Research Council, Medical Research Council, and European Community; R. M. is supported by a C. J. Martin Fellowship from NHMRC Australia; P. P. C. M. and J. N. B. are supported by the Ministry of Agriculture, Fisheries, and Food.

Received January 8, 1999; revised April 16, 1999.

References

Bacon, D., and Anderson, W.F. (1988). A fast algorithm for rendering space-filling molecule pictures. J. Mol. Graph. *6*, 219–220.

Bartlett, N.M., Gillies, S.C., Bullivant, S., and Bellamy, A.R. (1974). Electron-microscopy of reovirus reaction cores. J. Virol. *14*, 315–326.

Bourgeois, D., Nurizzo, D., Kahn, R., and Cambillau, C. (1998). An integration routine based on profile fitting with optimized fitting area for the evaluation of weak and/or overlapped two-dimensional Laue or monochromatic patterns. J. Appl. Crystallogr. *31*, 22–35.

Brünger, A.T. (1992). X-PLOR Version 3.1 (New Haven, CT: Yale University Press).

Burroughs, J.N., Grimes, J.M., Mertens, P.P.C., and Stuart, D.I. (1995). Crystallization and preliminary X-ray analysis of the core particle of bluetongue virus. Virology *210*, 217–220.

Chen, Z.G., Stauffacher, C., Li, Y., Schmidt, T., Bomu, W., Kamer, G., Shanks, M., Lomonossoff, G., and Johnson, J.E. (1989). Protein-RNA interactions in an icosahedral virus at 3.0 Å resolution. Science *245*, 154–159.

Delano, W.L., and Brünger, A.T. (1995). The direct rotation function—rotational Patterson correlation search applied to molecular replacement. Acta Crystallogr. D *51*, 740–748.

Dryden, K.A., Farsetta, D.L., Wang, G., Keegan, J.M., Fields, B.N., Baker, T.S., and Nibert, M.L. (1998). Internal structures containing transcriptase-related proteins in top component particles of mammalian orthoreovirus. Virology *245*, 33–46.

Eaton, B.T., Hyatt, A.D., and Brookes, S.M. (1990). The replication of bluetongue virus. Curr. Top. Microbiol. Immunol. *162*, 89–118.

Esnouf, R.M. (1997). An extensively modified version of MolScript that includes greatly enhanced coloring capabilities. J. Mol. Graph. *15*, 133–138.

Esnouf, R.M. (1999). Further additions to Molscript version 1.4, including reading and contouring of electron-density maps. Acta. Crystallogr. D *55*, 938–940.

Fisher, A.J., and Johnson, J.E. (1993). Ordered duplex RNA controls capsid architecture in an icosahedral animal virus. Nature *361*, 176–179.

Foulser, D. (1995). IRIS EXPLORER: a framework for investigation. Comp. Graphics *29*, 13–16.

French, S., and Wilson, K. (1978). On the treatment of negative intensity observations. Acta Crystallogr. A *34*, 517–525.

Gillies, S., Bullivant, S., and Bellamy, A.R. (1971). Viral RNA polymerases: electron microscopy of reovirus reaction cores. Science *174*, 694–696.

Grime, G.W., Dawson, M., Marsh, M., McArthur, I.C., and Watt, F. (1991). The Oxford submicron nuclear microscopy facility. Nucl. Instr. Methods Phys. Res. *B54*, 52–63.

Grimes, J.M., Burroughs, J.N., Gouet, P., Diprose, J.M., Malby, R., Mertens, P.P.C., and Stuart, D.I. (1998). The atomic structure of the bluetongue virus core. Nature *395*, 470–478.

Jacobs, B.L., and Langland, J.O. (1996). When two strands are better than one: the mediators and modulators of the cellular responses to double-stranded RNA. Virology *219*, 339–349.

Joklik, W.K. (1983). The reovirus particle. In The Reoviridae (New York: Plenum Press), pp. 9–78.

Joklik, W.K., and Roner, M.R. (1996). Molecular recognition in the assembly of the segmented reovirus genome. Prog. Nucleic Acid Res. Mol. Biol. *53*, 249–281.

Larson, S.B., Koszelak, S., Day, J., Greenwood, A., Dodds, J.A., and McPherson, A. (1993). Double-helical RNA in satellite tobacco mosaic-virus. Nature *361*, 179–182.

Lawton, J.A., Estes, M.K., and Prasad, B.V.V. (1997). Three-dimensional visualisation of mRNA release from actively transcribing rotavirus particles. Nat. Struct. Biol. *4*, 118–121.

Livolant, F., and Leforestier, A. (1996). Condensed phases of DNA: structures and phase transitions. Prog. Polym. Sci. *21*, 1115–1164.

Macfarlane, S.A., Shanks, M., Davies, J.W., Zlotnick, A., and Lomonossoff, G.P. (1991). Analysis of the nucleotide-sequence of bean pod mottle virus middle component RNA. Virology *183*, 405–409.

Matthews, B.W. (1968). Solvent content of protein crystals. J. Mol. Biol. *33*, 491–497.

Merritt, E.A., and Murphy, M.E.P. (1994). Raster3D version 2.0. A program for photorealistic molecular graphics. Acta Crystallogr. D *50*, 869–873.

Mertens, P.P.C., Burroughs, J.N., and Anderson, J. (1987). Purification and properties of virus particles, infectious subviral particles, and cores of bluetongue virus serotypes 1 and 4. Virology *157*, 375–386.

Mertens, P.P.C., Burroughs, J.N., Wade-Evans, A.M., Le Blois, H., Oldfield, S., Basak, A., Loudon, P., and Roy, P. (1992). Analysis of guanyltransferase and transmethylase activities associated with bluetongue virus cores and recombinant baculovirus-expressed core-like particles. In Bluetongue, African Horse Sickness, and Related Orbiviruses: Proceedings of the Second International Symposium, T.E. Walton and B.I. Osburn, eds. (Paris: CRC Press), pp. 404–415.

Namba, K., Pattanayek, R., and Stubbs, G. (1989). Visualization of protein-nucleic acid interactions in a virus. Refined structure of intact tobacco mosaic virus at 2.9 Å resolution by X-ray fiber diffraction. J. Mol. Biol. *208*, 307–325.

Otwinowski, Z., and Minor, W. (1997). Processing of X-ray diffraction data collected in oscillation mode. In Macromolecular Crystallography, J.W. Carter, Jr. and R.M. Sweet, eds. (San Diego: Academic Press), pp. 307–326.

Payne, C.C., and Mertens, P.P.C. (1983). Cytoplasmic polyhedrosis viruses. In The Reoviridae, W.K. Joklik, ed. (New York: Plenum Press), pp. 425–504.

Prasad, B.V.V., Rothnagel, R., Zeng, C.Q.-Y., Jakana, J., Lawton, J.A., Chiu, W., and Estes, M.K. (1996). Visualisation of ordered genomic RNA and localisation of transcriptional complexes in rotavirus. Nature *382*, 471–473.

Qiao, X., Qiao, J., and Mindich, L. (1997). Stoichiometric packaging of the three genomic segments of double-stranded RNA bacteriophage phi 6. Proc. Natl. Acad. Sci. USA *94*, 4074–4079.

Ramadevi, N., Burroughs, N.J., Mertens, P.P.C., Jones, I.M., and Roy, P. (1998). Capping and methylation of mRNA by purified recombinant VP4 protein of bluetongue virus. Proc. Natl. Acad. Sci. USA *95*, 13537–13542.

Rayment, I. (1983). Molecular replacement method at low resolution: optimum strategy and intrinsic limitations as determined by calculations on icosahedral virus models. Acta Crystallogr. A *39*, 102–116.

Ren, J., Esnouf, R., Garman, E., Somers, D., Ross, C., Kirby, I., Keeling, J., Darby, G., Jones, Y., and Stuart, D. (1995). High resolution structures of HIV-1 RT from four RT-inhibitor complexes. Nat. Struct. Biol. *2*, 293–302.

Roner, M.R., Sutphin, L.A., and Joklik, W.K. (1990). Reovirus RNA is infectious. Virology *179*, 845–852.

Roner, M.R., Lin, P.N., Nepluev, I., Kong, L.J., and Joklik, W.K. (1995). Identification of signals required for the insertion of heterologous genome segments into the reovirus genome. Proc. Natl. Acad. Sci. USA *92*, 12362–12366.

Roussel, A., Inisan, A.G., and Cambillau, C. (1991). TURBO-FRODO (Marseille, France: AFMB and Biographics).

Roy, P. (1989a). Bluetongue virus genetics and genome structure. Virus Res. *13*, 179–206.

Roy, P. (1989b). Bluetongue virus proteins. J. Gen. Virol. *73*, 3051–3064.

Shaw, A.L., Samal, S.K., Subramanian, K., and Prasad, B.V. (1996). The structure of aquareovirus shows how the different geometries of the two layers of the capsid are reconciled to provide symmetrical interactions and stabilization. Structure *4*, 957–967.

Smith, R.E., Zweerink, H.J., and Joklik, W.K. (1969). Polypeptide components of virions, top components and cores of reovirus type 3. Virology *39*, 791–810.

Stuart, D.I., Gouet, P., Grimes, J.M., Malby, R., Diprose, J.M., Zientara, S., Burroughs, J.N., and Mertens, P.P.C. (1998). Structural studies of orbivirus particles. Arch. Virol. *14*, 235–250.

Tsao, J., Chapman, M.S., Agbandje, M., Keller, W., Smith, K., Wu, H., Luo, M., Smith, T.J., Rossmann, M.G., Compans, R.W., and Parrish, C.R. (1991). The 3-dimensional structure of canine parvovirus and its functional implications. Science *251*, 1456–1464.

Tsuruta, H., Reddy, V., Wikoff, W., and Johnson, J. (1998). Imaging RNA and dynamic protein segments with low resolution virus crystallography: experimental design, data processing and implications of electron density maps. J. Mol. Biol. *284*, 1439–1452.

Wang, B.C. (1985). Resolution of phase ambiguity in macromolecular crystallography. In Diffraction Methods for Biological Macromolecules (Part B), H.W. Wyckoff, C.H.W. Hirs, and S.N. Timasheff, eds. (London: Academic Press Ltd.), pp. 90–117.

White, C.K., and Zweerink, H.J. (1976). Studies on the structure of reovirus cores. Selective removal of polypeptide lambda2. Virology *70*, 171–180.

Yazaki, K., and Miura, K. (1980). Relation of the structure of cytoplasmic polyhedrosis virus and the synthesis of its messenger RNA. Virology *105*, 467–479.

Zarbl, H., and Millward, S. (1983). The reovirus multiplication cycle. In The Reoviridae, W. Joklik, ed. (New York: Plenum Press), pp. 107–196.